

Surface Extraction from Multi-Material Components for Metrology using Dual Energy CT

Christoph Heinzl, Johann Kastner, and Eduard Gröller

Abstract— This paper describes a novel method for creating surface models of multi-material components using dual energy computed tomography (DECT). The application scenario is metrology and dimensional measurement in industrial high resolution 3D x-ray computed tomography (3DCT). Based on the dual source / dual exposure technology this method employs 3DCT scans of a high precision micro-focus and a high energy macro-focus x-ray source.

The presented work makes use of the advantages of dual x-ray exposure technology in order to facilitate dimensional measurements of multi-material components with high density material within low density material. We propose a workflow which uses image fusion and local surface extraction techniques: a prefiltering step reduces noise inherent in the data. For image fusion the datasets have to be registered. In the fusion step the benefits of both scans are combined. The structure of the specimen is taken from the low precision, blurry, high energy dataset while the sharp edges are adopted and fused into the resulting image from the high precision, crisp, low energy dataset. In the final step a reliable surface model is extracted from the fused dataset using a local adaptive technique.

The major contribution of this paper is the development of a specific workflow for dimensional measurements of multi-material industrial components, which takes two x-ray CT datasets with complementary strengths and weaknesses into account. The performance of the workflow is discussed using a test specimen as well as two real world industrial parts. As result, a significant improvement in overall measurement precision, surface geometry and mean deviation to reference measurement compared to single exposure scans was facilitated.

Index Terms—DECT image fusion, local surface extraction, Dual Energy CT, metrology, dimensional measurement, variance comparison.

1 INTRODUCTION

In state-of-the-art engineering the demands concerning the functionality of industrial components continuously increases the complexity of new parts. Furthermore the demands in terms of weight reduction, increased stability and new materials (*e.g.*, carbon-fibre-reinforced plastics) induce manufacturers to design new function-oriented and complex parts. In order to meet the requirements and specifications of construction drawings, manufacturing quality has to be assured using top of the line quality assurance techniques. Metrology (the science of measurement [30]) is used to study the surface geometry of a component, *e.g.*, distances, wall-thicknesses or diameters by means of coordinate measurements using tactile or optical sensors. This technology permits the calculations of surface dimensions at a calibrated precision over a defined measurement area.

In recent years the methodologies of metrology and dimensional measurement were expanded by introducing the novel technology of industrial 3D x-ray computed tomography (3DCT). 3DCT is an established method for visualization and for non-destructive-testing (NDT) of industrial components [5] and has recently gained importance in the area of dimensional measurement for industrial components. Figure 1 shows an image of the 3DCT at the Upper Austrian University of Applied Sciences - Wels Campus. The principle of 3DCT is to generate a series of x-ray attenuation measurements, which is used to produce a 3D grid of greyvalues corresponding to the spatial density distribution [9]. 3DCT provides full geometric information of a specimen including inner or hidden structures. A single scan non-destructively characterizes a specimen and detects material defects and geometri-

cal irregularities of the manufacturing process. Furthermore, the typical limitations of tactile and optical coordinate measurement technology can be avoided (*e.g.*, problems with deformable surfaces, reflecting glass probes). Industrial 3DCTs with cone beam geometry and flat panel detectors are prone to artefacts like noise-induced streaks, aliasing, beam-hardening, partial volume and scattered radiation effects [4]. Therefore the quality of the datasets is easily affected by the environmental conditions of the measurement. Some of the parameters which have a major contribution to the dataset's quality are: the specimen's geometry, the penetration lengths, the positioning of the specimen in the ray, the measurement parameters and the specimen's material combination.

Especially when scanning multi-material specimens with high differences in density and therefore in the attenuation coefficients of each

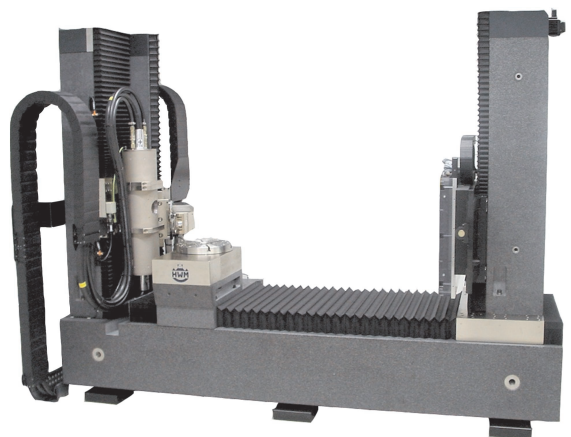


Fig. 1. 3D x-ray computed tomography system at the Upper Austria University of Applied Sciences - Wels Campus. General design of the CT: 225 keV and 450 keV x-ray sources are mounted on the left granite pillar, rotary plate for specimens, amorphous silicon matrix detector on the right granite pillar. A single 360 degree turn is sufficient to acquire the full geometry of a specimen.

- Christoph Heinzl is with Upper Austrian University of Applied Sciences, Wels Campus, E-mail: c.heinzl@fh-wels.at.
- Johann Kastner is with Upper Austrian University of Applied Sciences, Wels Campus, E-mail: j.kastner@fh-wels.at.
- Eduard Gröller is with Vienna University of Technology, Institute of Computer Graphics and Algorithms, E-mail: groeller@cg.tuwien.ac.at.

Manuscript received 31 March 2007; accepted 1 August 2007; posted online 27 October 2007. Published 14 September 2007.

For information on obtaining reprints of this article, please send e-mail to: tvcg@computer.org.

material, severe streaking artefacts prevent a reliable dimensional measurement. Usually, technicians in measurement technology disassemble the multi-material components. Each material is measured in a separate scan using optimal x-ray parameters. This procedure is time consuming and in several cases the specimen is destroyed. For instance, in the special case of a pressure sensor from the automotive industry, the sensor is cast integral into the plastic body and can not be removed without destroying the specimen. The common workflow for dimensional measuring of single-material industrial components can be summed up as follows: a prefiltering step reduces the reconstructed dataset's inherent noise in order to support surface detection. For common surface extraction tasks in industrial applications, usually a single isovalue is specified to distinguish between material and air [27]. A polygonal mesh is extracted along the selected isovalue using a surface creation algorithm (*e.g.*, marching cubes [15]). Finally the extracted surface model is compared to a computer aided design (CAD) model using variance comparison. The corresponding deviations between the reference and the test model are calculated and visualized by color-coding scalar deviations on the surface of the reference model.

Multi-material components with high density differences are not suitable for the common workflow of dimensional measurement using 3DCT. High density and highly absorbing materials (*e.g.*, steel) produce scattered radiation which is manifested in the reconstructed dataset. So the low absorbing material is simply covered by the different characteristics of artefacts from the strong absorbing material. If a global thresholding method for surface extraction is applied on an artefact affected dataset, holes and artificial structures will be introduced by different artefact types which modify the surface models. A reliable dimensional measurement is in most cases impossible. In Figure 2 and Figure 9 these circumstances are depicted.

To improve measurement results, recent research activities have tried to exploit Dual Energy Computed Tomography (DECT). By scanning a specimen using different energies and therefore different energy spectra of the x-ray source, it is possible to combine information of both reconstructions in order to quantify the different materials of a component.

This paper concentrates on designing a new workflow to facilitate dimensional measurements of multi-material components. The reconstructed datasets of both x-ray CT scans are adaptively fused on a regional basis and a valid surface model for dimensional measurement is locally determined. The major goal of our work is to design the workflow to follow typical dimensional measurement constraints. The method has to be applicable for typical dimensional mea-

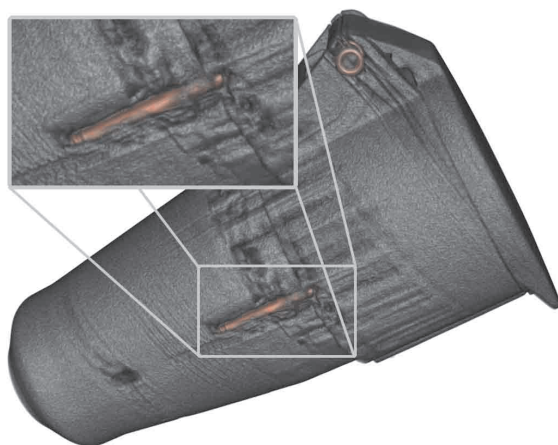


Fig. 2. Scattered radiation, beam hardening, and other physical effects produce severe artefacts, which modify the dataset and prevent a reliable global isosurface extraction. Artefacts manifest themselves as holes and artificial structures. In the rendering even a screw from the inside of the specimen becomes visible (high density objects are depicted in red, 3D view is rendered using raycasting).

surement tasks and practical in terms of quality and data-processing speed on commodity hardware. The reconstructed datasets of the two scans are taken as ground truth, assuming no additional information of CAD models or additional specifications of primitives (*e.g.*, cylinders, cuboids) in the scanned data. The special setup of the industrial 3DCT at the Upper Austrian University of Applied Sciences - Wels Campus is used to facilitate the DECT scans. In this setup a dual x-ray source design was created using a 450 keV macro focus source for the high energy scans and a 250 keV micro focus source for the high precision measurements.

2 RELATED WORK

2.1 Dual energy computed tomography

Concerning data acquisition in DECT there are two different techniques: the dual exposure / dual source and the dual (layer) detector technique [22].

Using the dual exposure / dual source technique a specimen is measured twice using different x-ray energies. Usually a high energy measurement and a low energy measurement are carried out successively without moving the specimen on the rotary plate. In order to combine both measurements either the position of the specimen is not changed between the measurements or an accurate registration of the datasets has to be performed. Major disadvantages of the dual exposure / dual source technique are the double measurement time and also the double storage requirement. However, in the area of industrial CT this method constitutes a novel enhancement for applications, which is usable on a widespread variety of existing 3DCTs.

Using the dual detector technique only a single measurement of the specimen is necessary. A modified detector consisting of two separate layers generates two penetration images: the front layer detects low energy photons and the back layer detects high energy photons. The disadvantage of this method is that the energy separation of these detectors is rather poor [22]. Application areas for this technique are the characterization of organic and inorganic materials in baggage control systems for airport security and the examination of drilling cores concerning material properties [7]. A considerable body of work on dual-energy 2D imaging is out of scope for our work and is therefore not treated.

Due to specifications of our 3DCT equipment the dual exposure / dual source technique was used for our DECT measurements.

2.2 Image Fusion

The general aim of image fusion is to combine a set of input images into a single output image. The output image preserves the salient information from each input image, suppresses noise and irrelevant parts of the input images, and should not generate distortions, artefacts, or inconsistencies [12]. Image fusion techniques are used in a wide range of applications, *e.g.*, medicine, remote sensing, industry, surveillance and defense applications which all benefit from the use of multiple images of a scene. Generally image fusion algorithms can be categorized into low, mid, and high levels. In some literature the levels are also referred to as pixel, feature, and symbolic levels.

Feature-based algorithms are usually more robust to signal-level noise compared to pixel-level algorithms. These algorithms typically segment the images into regions and fuse the regions using their various properties [12]. High-level fusion algorithms try to combine image descriptions, *e.g.*, in the form of relational graphs [31]. Feature and symbolic level fusion are out of scope for this work and are not considered any further.

In the area of pixel-level image fusion a considerable body of work has been done. Pixel-level algorithms work either in the spatial domain (*e.g.*, [13]) or in the transform domain (*e.g.*, [18]). Spatial-domain algorithms are able to focus on specific image areas limiting the influence of fusion in other areas. As transform domain algorithms create the fused image globally, undesirable artifacts may be created in several image areas while enhancing properties in others. For this reason transform domain algorithms are considered as not suitable in the proposed application area. Multiresolution analysis constitutes another branch of pixel-level fusion. Burt [1] created image pyramids by

applying filters with increasing spatial extent in order to separate information at different resolutions. The value with the highest saliency is taken at each position in the transform image, *e.g.*, using the intensity gradients as saliency measure [21]. Finally the fused image is created by an inverse transform of the composite image. Furthermore various wavelet transforms can be used to fuse images. The discrete wavelet transform [13],[14] and more recently, the dual-tree complex wavelet transform [18], [12] have been used in many applications to fuse images.

Multiresolution analysis turned out to produce suboptimal results in a difficult to tune and timeconsuming process. As we wanted to focus the fusion of the two datasets on edge regions, an adapted version of the weighted arithmetic image fusion is used. It employs a region based encoding of the weights for HE and LE dataset.

2.3 Local surface extraction

There are several methods in the area of industrial 3DCT that try to improve the surface extraction from industrial 3DCT data. Generally they can be grouped into two categories. In the first category the dataset is enhanced by artefact reduction [8] in order to generate a dataset with homogeneous greyvalues for each material. In this case, a single threshold is sufficient.

For techniques in the second category the underlying data is considered as ground truth and used for further processing. Whitaker et al. [29] introduced an approach that directly operates on voxel data. Based on the ideas of Sethian [24], this approach considers the zero level-set of a volume as a deformable surface. The surface is then deformed in order to minimize the mean curvature on the surface. Level-set evolution is computational expensive and timeconsuming on commodity hardware, and therefore undesirable for dimensional measurement tasks. Kindlmann and Durkin [10] take the data value as well as the gradient magnitude and the second derivative in order to design and explore a 3D transfer function space. Kniss et al. [11] have designed transfer function widgets that build on Kindlmann and Durkin's method. As Kindlmann and Durkin originally designed their method for volume visualization, the extraction of surface models is not included. Methods which extract surface models from binary data were proposed by Whitaker [28] and Gibson [2]. Whitaker proposed to change the constrained deformable surface model to a constrained level-set model, in order to create smooth models while bypassing the need for a separate surface representation. Gibson generates feature-preserving surface models by treating the binary input data as a constraining element in an energy-minimizing deformable surface system. In these methods, to a large extent the quality of the output depends on the prior segmentation, which would introduce another expensive step to the workflow. Heinzl et al. [3] proposed a pipeline which uses 3D image processing filters for preprocessing and segmentation of 3DCT datasets in order to create the surface model. In particular, after an edge preserving prefiltering step, a watershed filter is applied on the gradient magnitude image. The resulting binary segmented data is taken for the construction of a surface model using constrained elastic-surface nets. Due to segmentation of material regions, fine details might get lost and therefore measurement errors are introduced.

As the requested output of the workflow is a surface model, we apply a modified version of Steinbeiss's method [25] using a modified noise reduction scheme. This method locally adapts surface vertices to determine the best local surface position. Using an initial suitable surface model of the specimen, greyvalue profiles are calculated in the direction of each point's surface normal. The vertex location is then adjusted to correspond to the position with maximal gradient magnitude.

In this paper we describe a DECT workflow for surface extraction from multi-material components. We further discuss the results of applying the workflow to testparts as well as real world industrial components.

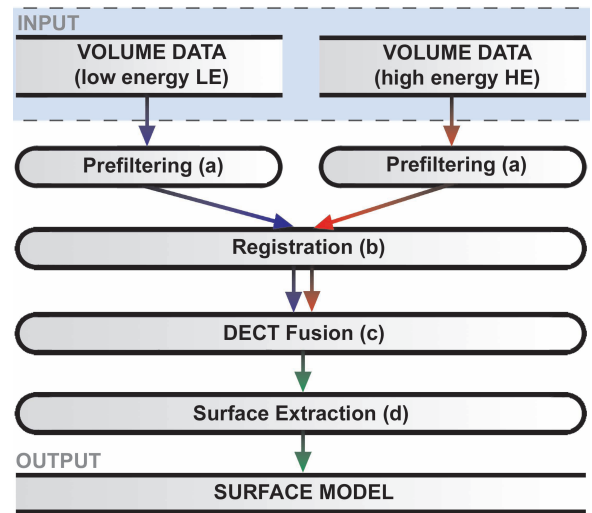


Fig. 3. DECT workflow for surface extraction from multi-material components; Input 1: Volume dataset from a low energy CT scan, Input 2: Volume dataset from a high energy CT scan; Output: Improved surface mesh.

3 DECT WORKFLOW FOR SURFACE EXTRACTION FROM MULTI-MATERIAL COMPONENTS

The basis of our approach is the dual source / dual exposure technology using a micro-focus and a macro-focus x-ray source. The high energy (HE) macro-focus CT scan generates nearly artefact-free but blurry, less precise and more noisy data. Usually macro-focus CT is the method of choice when examining large or high density components. Due to the higher energies used in macro-focus x-ray sources, the x-ray spot size (origin of the x-rays) is larger compared to micro-focus x-ray sources. It is approximately 2 mm versus 7 μm to 320 μm depending on the selected energy setting. The ideal case of a near punctiform x-ray source for an optimal projection image on the detector is abandoned in macro-focus CT in order to achieve higher penetration lengths. In contrast, the low-energy (LE) micro-focus measurement generates high precision but artefact affected data. The smaller x-ray spot size supports the generation of crisp and precise images, but the limited energy restricts penetration lengths.

Most of the approaches mentioned in the previous chapter are focused on a specific problem within the visualization pipeline. Our goal is to combine and extend existing methods according to the requirements of metrology. The workflow shall be applicable in every day use for dimensional measurements of multi-material components. As we do not have access to the projection images, the reconstructed volumes of the high energy (HE) and the low energy (LE) measurement are used as input. In the following subsections all components of the proposed DECT workflow including DECT fusion and local surface extraction are discussed in detail (see Figure 3).

3.1 Preprocessing

Due to the different characteristics in each of the two scanned datasets concerning artefacts and signal to noise ratio, a preprocessing step is essential. Both high energy (HE) and low energy (LE) datasets are affected to a certain degree by ambient noise, but especially the HE dataset has to be preprocessed to reduce noise due to a more intense noise level of the detector in the higher energy bands. In case of the LE dataset, the preprocessing step reduces the propagation of artefacts to subsequent steps of the workflow. The preprocessing is accomplished by applying anisotropic diffusion which was first proposed by Perona and Malik [20]. More recently, a comprehensive book on the topic of geometry-driven diffusion was edited by ter Haar Romeny [26]. Compared to isotropic smoothing, the characteristic of anisotropic diffusion filters is to smooth the data without blurring or moving edges. So the dataset's noise is reduced but specific image features are preserved.

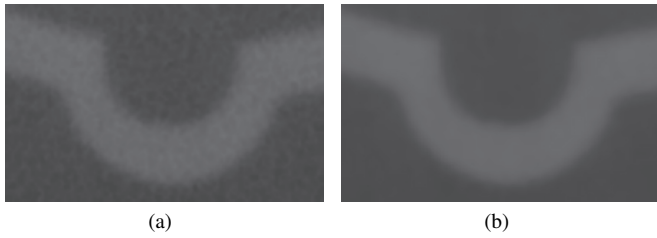


Fig. 4. Anisotropic-diffusion filter, axial cross section through a cutout of a 400V connector, before (a) and after (b) anisotropic diffusion filtering. Smaller artefacts are removed and the dataset's noise is decreased.

As these properties are desirable for dimensional measurement, Perona and Malik's anisotropic diffusion method is used in the DECT workflow. Initially, multi-scale descriptions of the input images are calculated. If an image $U(\mathbf{x})$ is embedded in a higher dimensional function of derived images $U(\mathbf{x}, t)$ then this higher dimensional function represents the solution of the heat diffusion equation,

$$\frac{dU(\mathbf{x}, t)}{dt} = \nabla \cdot C \nabla U(\mathbf{x}, t) \quad (1)$$

which is constrained by a constant conductance coefficient C and the initial condition $U(\mathbf{x}, 0) = U(\mathbf{x})$ representing the original image. If C is extended to a function of \mathbf{x} , the solution of the heat equation will then be

$$\frac{dU(\mathbf{x}, t)}{dt} = C(\mathbf{x}) \Delta U(\mathbf{x}, t) + \nabla C(\mathbf{x}) \nabla U(\mathbf{x}, t) \quad (2)$$

A variable conductance term C can now modify the way the diffusion process takes place. Typically, C is chosen as a function of image features. This allows selectively preserving or removing features by anisotropically varying the diffusion strength. Specifying C as a non-negative monotonically decreasing function as in

$$C(\mathbf{x}) = e^{-\left(\frac{\|\nabla U(\mathbf{x})\|}{K}\right)^2}, \quad K = \text{const} \quad (3)$$

will force the diffusion to mainly take place in homogeneous interior regions without affecting boundary regions [6]. When applying an anisotropic-diffusion filter, the dataset's inherent noise can be significantly reduced without losing edge information. Scattered radiation effects are removed without blurring edges. This is essential for surface detection (see Figure 4).

3.2 Registration

When measuring a specimen using different x-ray source setups of the CT scanner, slight changes in the positioning and the orientation of the specimen in the dataset may occur. To avoid the propagation of this error, a registration procedure has to be applied. In the DECT workflow the high energy (HE) dataset is considered as the fixed image, as it is robust to artefacts. The low energy (LE) dataset is considered as the moving image which is registered to the fixed image. In order to improve the performance of the registration algorithm with regard to speed and accuracy a multi-resolution approach is commonly used. The fixed image and the moving image are decomposed into image pyramids, which downsample the images level by level. Starting at the top level of the pyramids the coarsest images of the two pyramids are registered to each other. The registration is refined with each of the succeeding image levels. This guarantees a high robustness of the registration procedure.

In order to ensure the flexibility of using scans from different 3D imaging modalities, a mutual information approach is used. To compute the mutual information between the fixed (HE) and the moving image (LE) the method of Mattes et al. [16], [17] is used. This method evaluates the marginal and joint probability density function (PDF) at discrete positions (bins) which are uniformly spread within the dynamic range of the images. The entropy values are calculated by summing over the bins. Using this approach the fixed image PDF does not

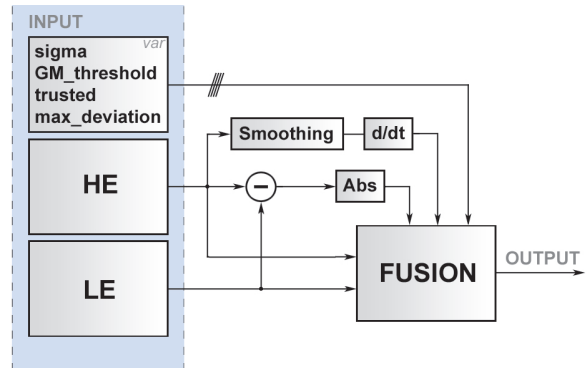


Fig. 5. Principle of DECT fusion: The fusion of the LE and the HE input is performed at edge regions of the HE dataset which are defined by the gradient magnitude. The contribution of each dataset is linearly weighted according to the absolute-value difference between the two images. To avoid misclassifications of artefacts the absolute value difference is limited.

need to be smooth, because it does not contribute to the derivatives. A zero order (box car) B-Spline kernel is used for the fixed image intensity PDF. To ensure smoothness, the moving image intensity PDF is computed with a third order B-Spline kernel.

3.3 DECT fusion

Due to the higher energies of our high energy (HE) macro-focus x-ray source, the main object structure of the considered specimens is depicted best in the HE dataset. However, the larger x-ray spot size of the macro-focus x-ray source generates more blurred edges in the datasets. In contrast, the small x-ray spot size of our micro-focus source supports to create crisp and precise images. The limited energy restricts penetration lengths and therefore severe artefacts are induced in the low energy dataset. The severe artefacts in the LE dataset change their characteristics and orientation according to the measurement parameters and the positioning of the specimen in the x-ray beam.

In order to combine the advantages of both measurements, the main object structure from the HE dataset is fused with the crisp edges of the LE dataset. As common image fusion methods as well as multiresolution analysis turned out to be inefficient or suboptimal, we developed a DECT specific approach for image fusion (see Figure 5). To determine the edge regions, a gradient magnitude image is extracted by applying a Gaussian filter kernel with a user defined σ followed by a gradient magnitude filter. The thresholding of the smoothed gradient magnitude image allows the specification of edge regions. Only the edge regions above a user defined level ($GM_threshold$) are considered for fusion. To detect artefact affected regions, an absolute-value difference-image between the HE and the LE measurements is computed. Especially in artefact affected regions and also in the edge regions, major deviations are depicted in the difference image.

Subsequently the datasets are combined by local arithmetic image fusion. In this step the contribution of each dataset is linearly weighted according to the absolute value difference between the two images. To avoid misclassifications of artefacts the absolute-value difference is limited by $max_deviation$. Finally, for trusted regions of low difference in the greyvalues of the LE and the HE data, a $trusted$ level is defined. Within the trusted level the LE dataset is weighted with 100%. For the effect of arithmetic image fusion see Figure 6.

3.4 Local surface extraction

For surface determination we use a local surface extraction approach [25]. First a reliable global isosurface is extracted from the fused dataset. It includes the topology of the underlying data but still contains inhomogeneities and errors due to the local varying characteristics of the greyvalues. To correct these misclassifications, each surface vertex is moved in the direction of the surface normal. The vertex location is moved along the normal until the gradient magnitude

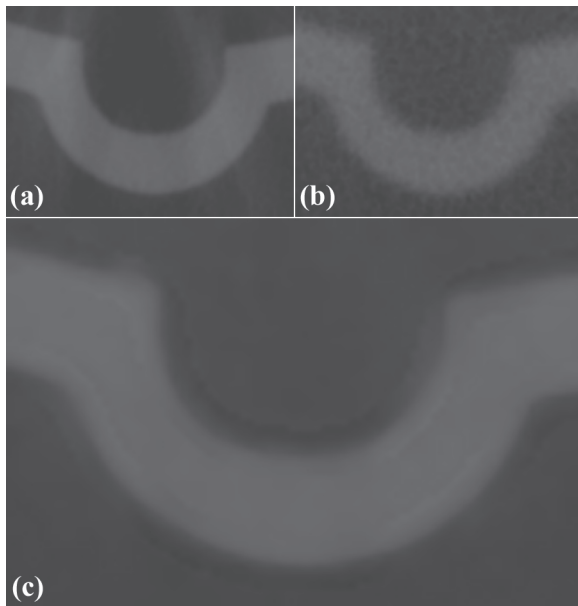


Fig. 6. Axial cross section through a cutout of a 400V connector. LE image (a), HE image (b) and fused image (c). Using our image fusion approach the edges are significantly enhanced for surface extraction without keeping artefacts from the LE dataset.

reaches its maximum. This is accomplished by trilinear interpolation of the greyvalues along the surface normal and computing the derivative of the generated greyvalue profile. As a constraint, a user-defined maximum distance for the repositioning of a vertex is used (P_{origin} , P_{end}). The local modification of vertices with predefined constraints produces a surface model with improved precision. To reduce repositioning failures due to noise, not only the density profile along the normal is taken into account, but also close-by profiles along directions parallel to the normal. In the tangent plane to the normal direction, a 3×3 neighborhood is used to compute 9 density profiles (see Figure 7). The directional derivative along each profile is estimated according to $f'(\mathbf{x}) = f(\mathbf{x}) - f(\mathbf{x} - 1)$, where \mathbf{x} and $\mathbf{x} - 1$ are successive positions along the profile. For each of the nine profiles the position with the maximal gradient magnitude is determined. The improved edge location is calculated by using either a local weighted mean or the median position.

4 RESULTS AND DISCUSSION

For all specimens high absorbing material is covered by low absorbing material. All CT scans were performed on a HWM RayScan 250E system with a 225 keV micro-focus and a 450 keV macro-focus x-ray

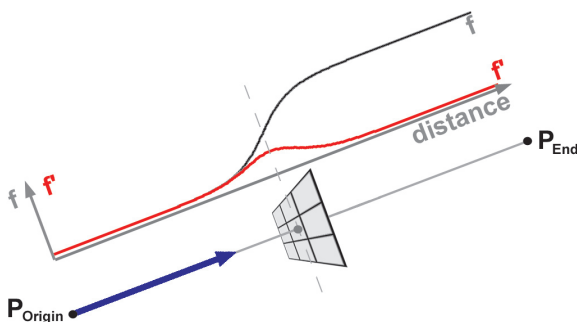


Fig. 7. Local surface extraction adapts the surface model by moving surface vertices in the direction of the corresponding point normal to a position with maximum gradient magnitude. The dataset's noise is accommodated by considering the neighborhood of a surface point candidate.

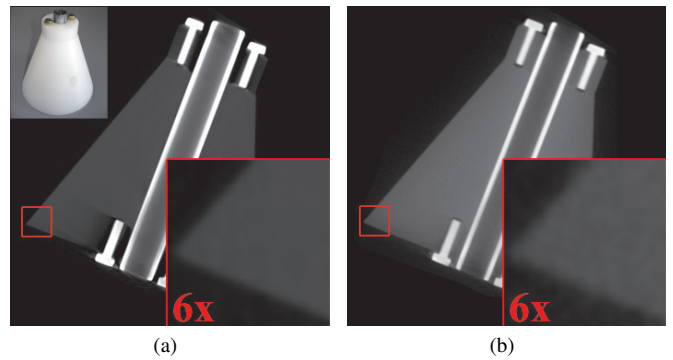


Fig. 8. Specimen one: Polyethylene testpart. An axial cross section of micro-CT scan (a) shows severe artefacts in the area of the metallic screws. Artefacts are the dark areas around the screws. Image (b) shows a cross section of the macro-CT scan. Compared to the LE scan the HE scan is less artefact affected but less precise and contains more noise. The detail images show a 6x zoom of the edge region (marked in red).

Table 1. Parameters for specimen one (PE testpart)

Parameter	Specimen one HE	Specimen one LE
projections	900	900
voltage (kV)	440	200
current (μA)	1300	450
integration time (ms)	2000	1000
prefiltering	1 mm W + 1.5mm Cu	1mm Cu
datasize	508*523*611	508*523*611
voxelsize (μm)	200	200

source. For the micro-focus setup the best achievable resolution is $7 \mu\text{m}/\text{voxel}$ depending on the maximum dimension of the specimen. For the macro-focus setup the best achievable resolution is $150 \mu\text{m}/\text{voxel}$. All datasets are stored in 16 bit unsigned short. Reference measurements were performed on a Zeiss SPECTRUM 700 (ST3/RDS-RST) Vast XXT coordinate measuring machine with a longitudinal measurement error of $2.2 \mu\text{m} \cdot \frac{\text{length}}{300}$. Our demo application was implemented in Visual C++ using ITK [6] and VTK [23]. For evaluation of deviations the commercial tools Raindrop Geomagic Qualify 7 and Carl Zeiss Calypso are used.

4.1 Specimens

4.1.1 Polyethylene testpart

Specimen one (Figure 8) is a homogeneous polyethylene (PE) testpart used for analysis of parameter variations in dimensional measurement. The PE testpart consists of a cone with an attached cylinder. Six smaller vertical drill holes are placed on the bottom and top side, four in the base of the specimen and two on top. Together with the central drill these features are serving to determine the exactness of a scan by evaluating distances and dimensions of the holes. A round steel bar is positioned in the major central drill and steel screws are placed and fixed in the drill holes, which makes this part a multi-material object. The PE testpart was measured twice without moving the specimen but using different x-ray source setups. The first measurement was a high energy (HE) macro-focus scan in order to determine the structure of the specimen. The second measurement was a low energy (LE) high precision micro-focus scan. For detailed CT measurement parameters see Table 1.

4.1.2 400 Volt connector

Specimen two (Figure 9) is a 400 Volt power connector according to the European IEC 60309 system. This component consists of a plastic housing, five power pins, two steel screws to connect the housing

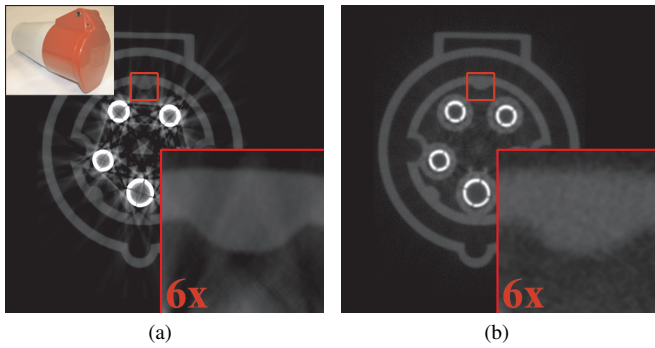


Fig. 9. Specimen two: 400 Volt connector. An axial cross section of the low energy micro-CT scan (a) shows the typical artefacts within multi-material components due to too low x-ray energies: Starting from the pins severe streaking artefacts exist. Using the high energy macro-CT scan, most of the streaking artefacts can be removed (b) but the edges are more blurry (see detail images).

Table 2. Parameters for specimen two (400 Volt connector)

Parameter	Specimen two HE	Specimen two LE
projections	1080	1440
voltage (kV)	440	210
current (μ A)	1000	680
integration time (ms)	1000	1000
prefiltering	1 mm W + 1.5 mm Cu	2 mm Cu
datasize	391*552*847	391*552*847
voxelsize (μ m)	171	171

parts, two steel-screws for the strain relief of the power cable, a spring and a bearing for the cap mechanism. Figure 2 shows a 3D rendering of a micro-focus CT scan of specimen two. This specimen shows severe artefacts around the power pins. Greyvalue modifications due to scattered radiation of the metal components exceed the plastic's greyvalue. CT measurement parameters are listed in Table 2.

4.1.3 Terminal block

Specimen three (see Figure 10) is a terminal block from home automation systems. Terminal blocks are widely used, providing a convenient means of connecting electrical wires. This part is built using a plastic body, which acts as a carrier for the metal clamps, a spring, which fixes the terminal on the top hat rail, and finally the two metal clamps

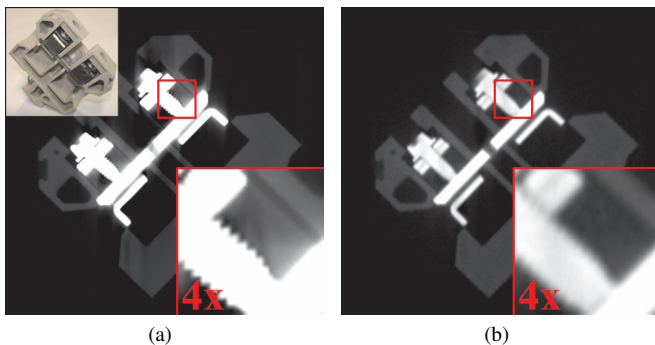


Fig. 10. Specimen three: Terminal block. In the cross section of the micro-CT scan (a) streaking artefacts around the metallic clamps are present. Image (b) shows the cross section of the macro-CT scan. In the area of the screws the disadvantages of the macro-focus CT are revealed: Fine structures disappear (see detail images).

Table 3. Parameters for specimen three

Parameter	Specimen three HE	Specimen three LE
projections	1080	1080
voltage (kV)	400	160
current (μ A)	2200	660
integration time (ms)	1000	2000
prefiltering	1 mm W + 1.5 mm Cu	2 mm Cu
datasize	88*322*324	88*322*324
voxelsize (μ m)	200	200

holding the wires, which are connected by the power rail. This representative multi-material component was chosen because of its regular structure and a convenient geometry for coordinate measurement machines (CMM). In total, 16 inspection features of the object were specified to calculate the dimensional deviation to a CMM reference measurement. The CT measurement parameters for the terminal block are listed in Table 3.

4.2 Tuning the DECT workflow

To produce reliable surface models for dimensional measurement, the parameter settings for each step are essential. As prefiltering step an anisotropic diffusion filter (Figure 3a) is used, which creates a more homogeneous dataset without modifying edge information. This step is crucial especially for the LE dataset in order to reduce noise and smaller artefacts. The aim of prefiltering is to improve the information to be fused. The noisier a dataset is, the more iterations of the diffusion filter have to be applied. The conductance C (equation 3) controls the local degree of smoothing and the areas to be smoothed. The higher the conductance, the more the diffusion filter acts like an isotropic filter, smoothing all regions. The smaller the conductance, the more features are preserved. As we do not want to preserve artefacts a rather high setting of the conductance is used for the LE dataset and an even higher setting for the HE dataset. For the LE dataset, a parameter setting of at least 5 iterations and a conductance of 10-50 turned out to produce reliable results. For the HE measurement we used 10 iterations at a slightly higher conductance of 75 to compute a smoother dataset.

In the registration step (Figure 3b) the HE dataset is considered as fixed image and the LE dataset as moving image. For the image pyramids a fixed setting of five levels is used.

For the DECT image fusion (Figure 3c) the gradient image of the Gaussian smoothed HE datasets determines the fusion regions. The wider these edge regions are, the smoother the image fusion will adopt features of the LE dataset. Using a sigma value of at least 0.2, a blurry image of the HE dataset is generated. When applying a gradient magnitude filter on this input image, a smooth gradient image is obtained. Depending on the dataset and the quality of edges, an edge image is produced with a smooth increase and decrease of the gradient magnitudes. The width of a typical edge is supposed to be approximately 5 to 10 voxels wide for a smooth image fusion. The trusted level which weights the LE dataset with 100% should not exceed the standard deviation of the HE dataset. Otherwise artefacts are transferred to the resulting image.

In the local surface extraction step (Figure 3d) a reliable surface model is extracted using a global threshold. For the locally improved surface mesh gradient magnitudes along the surface normal have to be evaluated. The number of samples and the maximum sample distance have to be specified. The finer the sampling rate, the finer the positioning of the surface vertices. Generally settings of up to 50 samples within voxelsize are a valuable compromise between computation time and accuracy. A more difficult parameter is the maximum sample distance, which serves as a constraint for the repositioning of vertices. Exceeding a maximum sample distance of 5 times the voxelsize may produce erroneous results due to imprecise oriented surface normals of the isosurface. Usually settings of 2 to 5 times the voxelsize produce a reliable improved surface mesh. Finally the normal orientation (pos-

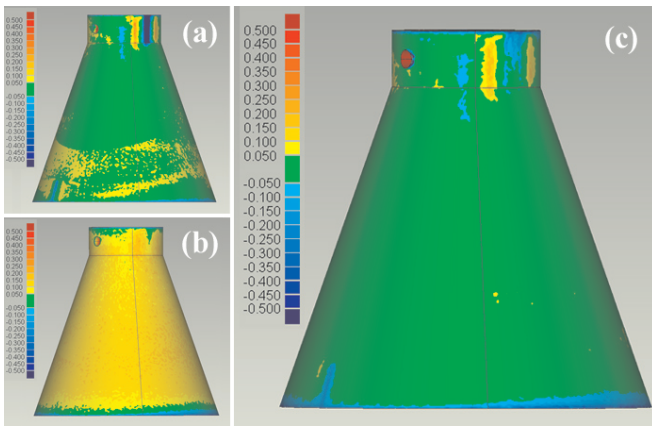


Fig. 11. Variance comparison of specimen one between CAD model and extracted surface models. Deviations are colorcoded using the same scale. (a) shows the variance comparison using a global threshold applied to the LE dataset and in (b) to the HE dataset. The result when applying the DECT workflow to specimen one is depicted in (c). Artefacts of the LE measurement can be avoided to a high extent. The smoother characteristic of the DECT surface is indicated by the large low deviation area (green).

itive, negative or both directions) is also a parameter to be set. Due to the noise in the surface mesh considering the use of both directions produces the most reliable results.

4.3 Evaluation of DECT workflow results

To get an overview of deformations throughout the whole specimen compared to reference geometry data, *e.g.*, a CAD model, variance comparisons are widely used. A common visualization method for variance comparison is color coding the reference's surface corresponding to the local deviation. To show the different results of generating surface models, variance comparisons between the CAD model and three surfaces are depicted. The first surface is due to the best global threshold from the LE data. The second surface is due to the best global threshold from the HE data. The third surface is the result of our proposed DECT workflow. Note: the CAD model does not contain the data of the screws and the round bar. The best global thresholds are empirically determined. The metal parts are intended to show the loss in data quality when placing high absorbing components within low absorbing material and to produce deformations in the iso-surface due to artefacts. In Figure 11a, high deviations due to streaking artefacts and scattered radiation are depicted in dark red and dark blue. In less artefact affected areas, a high correspondence between the CAD model and LE measurement can be seen. Figure 11b shows a more homogeneous distribution of deviations. For the HE measurement, the mean deviation is much higher but hardly any strong artefacts affect the surface. Applying the DECT workflow the advantages of both measurements can be combined. The variance comparison shows higher accuracy than the HE dataset while reducing artefacts of the LE dataset (see Figure 11c). In the DECT result not all artefacts could be removed because the trusted level was set to the standard deviation of the HE dataset and therefore these deviations were considered to be real. Using a lower trusted level would introduce a part of the HE datasets noise.

Specimen two was chosen to demonstrate the DECT workflow's ability to produce reliable surface models without holes. The multi-material characteristics of this specimen produce streaking artefacts and scattered radiation in the reconstructed dataset. These circumstances are depicted in Figure 2 and 9. When extracting an isosurface from the LE dataset, common methods like Otsu's method [19] turned out to produce unusable results. The best global threshold to create a surface model was determined again empirically. However, a complete and reliable measurement is impossible due to severe artefacts of the derived surface model (Figure 12a). Using the HE dataset of spec-

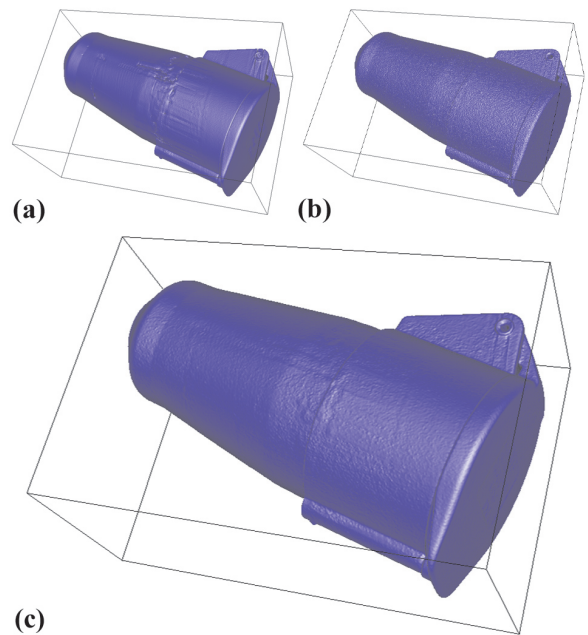


Fig. 12. Surface extraction of specimen two using a global threshold applied on the LE dataset (a) and on the HE dataset (b). The result when applying the DECT workflow on specimen two is depicted in (c). Artefacts of the LE measurement can be avoided. The coarse structure and the higher mean deviation of the HE measurement was significantly reduced. DECT fusion even preserves fine details of the LE dataset like the sticker on the jacket of the 400 V connector or the imprint on the cap (see red arrows).

imen two, a reliable surface model may be extracted but due to the larger focal spot of the macro-focus source fine details get lost. Furthermore due to the much higher ambient noise level of the HE dataset, the generated surface model has a rather coarse surface structure (see Figure 12b).

When applying the DECT workflow, part of the details are reconstructed by incorporating details from the LE dataset. In the resulting surface model holes were removed, surface deformations through scattered radiation were avoided and fine details were fused into the resulting dataset (see Figure 12c). For specimen two, slight deformations in the surface can be seen which is again due to a compromise between introduction of the HE dataset's noise and adoption of artefacts from the LE dataset.

Specimen three was chosen as another representative multi-material component to demonstrate the performance of the DECT workflow. Dimensional measurement accuracies are verified by specification and evaluation of 16 inspection features (3 diameters of cylinders and 13 distances). As reference, specimen three was measured using a high precision coordinate measuring machine. In order to point out the differences in dimensional measurement, the same features were evaluated in the LE measurement, the HE measurement and the resulting dataset of the DECT workflow using Calypso. As expected, the LE measurement produces a result with higher precision than the HE measurement. In comparison to the LE dataset the HE measurement is less artefact affected. Applying the DECT workflow, artefacts are reduced, which can be seen in the lower mean deviation per inspection feature. For specimen three the mean deviation per inspection feature can be lowered by more than 1/3 taking the DECT workflow compared to using the LE dataset and nearly 1/2 compared to using the HE dataset (see Table 4 for details).

5 SUMMARY AND CONCLUSIONS

A novel workflow for dimensional measurement of multi-material industrial components is presented, allowing reproducible and robust

Table 4. Mean deviations per inspection feature for specimen three

	LE		HE		DECT		
	(mm)	(%)	(mm)	(%)	(mm)	(%)	
overall mean	16	0.0251	0.25	0.0299	0.31	0.0158	0.16
diameters mean	3	0.0309	0.52	0.0402	0.75	0.0206	0.37
lengths mean	13	0.0238	0.19	0.0275	0.21	0.0147	0.11

surface extraction. The introduced DECT workflow exploits a dual source / dual exposure approach of dual energy computed tomography. It facilitates dimensional measurement of artefact affected datasets from multi-material components. The presented DECT workflow combines the advantages of dual x-ray exposure technology by taking two x-ray CT datasets with complementary strengths and weaknesses into account. The workflow integrates image fusion and local surface extraction techniques: After prefiltering both datasets are registered to each other. In the fusion step, the two scans are combined by integrating the low energy (LE) dataset's accuracy with the high energy (HE) dataset's robustness. Finally, a reliable surface model is extracted using a local adaptive technique.

The accuracy and the applicability of the DECT workflow has been discussed using a testpart as well as two industrial components. Results are depicted in variance comparisons, reliable surface models, and quantitative measurement errors. For the terminal block, the mean deviation per inspection feature could be decreased by a third compared to using the LE dataset and nearly a half compared to using the HE dataset.

A major aim of our future work is to further improve the quality of image fusion. The exploitation of different imaging modalities for metrology will be another topic in the future.

ACKNOWLEDGEMENTS

The presented work has been funded by the FH-Plus project "Zerstörungsfreie und In-situ-Charakterisierung von Werkstücken und Materialien unter besonderer Berücksichtigung von Brennstoffzellen" (see <http://www.fh-wels.at> and <http://www.3dct.at>) of the Austrian Research Promotion Agency (FFG). Furthermore this work is partly supported by the PVG project, Austrian Science Fund (FWF) grant no P18547. Thanks to the vis-group of the Vienna University of Technology, Institute of Computer Graphics and Algorithms, for support in designing this method and the CT group of the Upper Austrian University of Applied Sciences - Wels Campus for CT measurements, reference measurements and illustrations.

REFERENCES

- [1] P. J. Burt. The pyramid as a structure for efficient computation. In A. Rosenfeld, editor, *Multiresolution Image Processing and Analysis*, pages 6–35. Springer-Verlag, 1984.
- [2] S. F. Gibson. Constrained elastic surface nets: generating smooth surfaces from binary segmented data. In *MICCAI '98: Proceedings of the First International Conference on Medical Image Computing and Computer-Assisted Intervention*, pages 888–898, 1998.
- [3] C. Heinzl, R. Klingsberger, J. Kastner, and E. Gröller. Robust surface detection for variance comparison. In *Proceedings of Eurographics/IEEE-VGTC Symposium on Visualisation*, pages 75–82, 2006.
- [4] J. Hsieh. *Computed Tomography: Principles, Design, Artifacts and Recent Advances*. SPIE-The International Society for Optical Engineering, 2003.
- [5] R. Huang, K.-L. Ma, P. McCormick, and W. Ward. Visualizing industrial CT volume data for nondestructive testing applications. In *VIS '03: Proceedings of the 14th IEEE Visualization 2003 (VIS'03)*, pages 547–554, 2003.
- [6] L. Ibanez, W. Schroeder, L. Ng, and J. Cates. *The ITK Software Guide*. Kitware, Inc. ISBN 1-930934-10-6, <http://www.itk.org/ItkSoftwareGuide.pdf>, first edition, 2003.
- [7] M. Iovea, O. Dului, G. Oaie, C. Ricman, and G. Mateiasi. Dual-energy computer tomography and digital radiography investigation of organic and inorganic materials. In *Proceedings of European Conference on Non Destructive Testing*, 2006.
- [8] S. Kasperl. *Qualitätsverbesserungen durch referenzfreie Artefaktreduzierung und Oberflächennormierung in der industriellen 3D-Computertomographie*. PhD thesis, Technische Fakultät der Universität Erlangen Nürnberg, 2005.
- [9] J. Kastner, E. Schlothauer, P. Burgholzer, and D. Stifter. Comparison of x-ray computed tomography and optical coherence tomography for characterisation of glass-fibre polymer matrix composites. In *Proceedings of World Conference on Non Destructive Testing*, pages 71–79, 2004.
- [10] G. Kindlmann and J. W. Durkin. Semi-automatic generation of transfer functions for direct volume rendering. In *IEEE Symposium on Volume Visualization*, pages 79–86, 1998.
- [11] J. Kniss, G. Kindlmann, and C. Hansen. Interactive volume rendering using multi-dimensional transfer functions and direct manipulation widgets. In *VIS '01: Proceedings of the conference on Visualization '01*, pages 255–262, Washington, DC, USA, 2001. IEEE Computer Society.
- [12] J. J. Lewis, R. J. OCallaghan, S. G. Nikolov, D. R. Bull, and C. N. Canagarajah. Region-based image fusion using complex wavelets. In *Proceedings of the Seventh International Conference on Information Fusion*, volume 1, pages 555–562, 2004.
- [13] H. Li, B. S. Manjunath, and S. K. Mitra. Multisensor image fusion using the wavelet transform. In *Image Processing, 1994. Proceedings. ICIP-94., IEEE International Conference*, volume 1, pages 51–55, 1994.
- [14] Y. O. L.J. Chipman and L. Graham. Wavelets and image fusion. In *Proceedings of the International Conference on Image Processing*, pages 248–251, 1995.
- [15] W. Lorensen and H. Cline. Marching cubes: a high resolution 3D surface construction algorithm. In *ACM SIGGRAPH Computer Graphics*, volume 21, pages 163–169, 1987.
- [16] D. Mattes, D. R. Haynor, H. Vesselle, T. Lewellen, and W. Eubank. Non-rigid multimodality image registration. In *Medical Imaging 2001: Image Processing*, pages 1609–1620, 2001.
- [17] D. Mattes, D. R. Haynor, H. Vesselle, T. Lewellen, and W. Eubank. PET-CT image registration in the chest using free-form deformations. In *IEEE Transactions in Medical Imaging*, volume 22, pages 120–128, 2003.
- [18] S. Nikolov, P. Hill, D. Bull, and C. Canagarajah. *Wavelets in Signal and Image Analysis*, chapter Wavelets for image fusion, pages 213–244. Kluwer Academic Publishers, The Netherlands, 2001.
- [19] N. Otsu. A threshold selection method from grey level histograms. In *IEEE Transactions on Systems, Man, and Cybernetics*, volume 9, 1979.
- [20] P. Perona and J. Malik. Scale-space and edge detection using anisotropic diffusion. In *IEEE Transactions on Pattern Analysis and Machine Intelligence*, volume 12, pages 629–639, 1990.
- [21] V. Petrovic and C. Xydeas. Gradient-based multiresolution image fusion. In *IEEE Transactions on Image Processing*, volume 13, pages 228–237, 2004.
- [22] V. Rebuffel and J.-M. Dinten. Dual-energy x-ray imaging: benefits and limits. In *Proceedings of European Conference on Non Destructive Testing*, 2006.
- [23] W. Schroeder, K. Martin, and B. Lorensen. *The Visualization Toolkit*. Kitware, Inc., 2004.
- [24] J. Sethian. *Level Set Methods and Fast Marching Methods: Evolving Interfaces in Computational Geometry, Fluid Mechanics, Computer Vision and Materials Sciences*. Cambridge University Press, second edition, 1999.
- [25] H. Steinbeiss. *Dimensionelles Messen mit Mikro-Computertomographie*. PhD thesis, Technische Universität München, 2005.
- [26] B. M. ter Haar Romeny. *Geometry Driven Diffusion in Computer Vision. Series on Computational Imaging and Vision*. Kluwer Academic Publishers, Dordrecht, the Netherlands, 1994.
- [27] VolumeGraphics. *VG Studio Max 1.2 - User's Manual*. 2004.
- [28] R. T. Whitaker. Reducing aliasing artifacts in iso-surfaces of binary volumes. In *VVS '00: Proceedings of the 2000 IEEE Symposium on Volume visualization*, pages 23–32, 2000.
- [29] R. T. Whitaker and D. E. Breen. Level-set models for the deformation of solid objects. In *The third international workshop on implicit surfaces*, pages 19–35, 1998.
- [30] Wikipedia. Metrology. Wikipedia: WWW: <http://en.wikipedia.org/wiki/Metrology>, March 18th 2007.
- [31] M. L. Williams, R. C. Wilson, and E. R. Hancock. Deterministic search for relational graph matching. *Pattern Recognition*, 32(7):1255–1271, 1999.